
ROTATIONAL DYNAMICS INDUCED BY LOW-ENERGY BINARY COLLISIONS OF QUANTUM DROPLETS

A PREPRINT

J. E. Alba-Arroyo, S. F. Caballero-Benitez, R. Jáuregui *

Departamento de Física Cuántica y Fotónica,
 Laboratorio de Simulaciones Computacionales para Sistemas Cuánticos (LSCSC)
 Laboratorio Nacional de Materia Cuántica (LANMAC),
 Instituto de Física, Universidad Nacional Autónoma de México, Ciudad de México C.P. 04510,
 *rocio@fisica.unam.mx

August 15, 2023

ABSTRACT

A theoretical analysis of the rotational dynamics induced by off-axis binary collisions of quantum droplets constituted by ultracold atoms is reported. We focus on quantum droplets formed by degenerate dilute Bose gases made from binary mixtures of alkaline atoms under feasible experimental conditions. The stability of the ground state is known to be longer for the chosen heteronuclear gases than for the homonuclear ones. In both cases, we find that the dynamics seem to privilege high similarity of the density of each atomic species. However, the evolution of the phase of the corresponding order parameter differs significantly for heteronuclear admixtures. We evaluate the fidelity as a figure of merit for the overlap between the order parameters of each atomic species. Dynamical evidence of the differences between the phases of the order parameters is predicted to manifest in their corresponding linear and angular momenta. We numerically verify that the total angular and linear momenta are both conserved during the collision. Some direct correlations between the Weber number and the impact parameter with the distribution of the dynamical variables are established.

1 Introduction

Self-bound droplets formed in ultracold atomic Bose gases were recently predicted [1, 2] and experimentally observed [3, 4, 5, 6]. The stabilization of quantum droplets in binary mixtures of ultracold atoms arises from a calibrated competition between interspecies attractive interactions and intraspecies repulsive interactions. The proper description of this regime requires the incorporation of quantum fluctuations, i.e., beyond mean-field effects. They involve either direct extensions of the Lee–Huang–Yang (LHY) formalism [7] to binary mixtures [8] or its analogue for dipolar interactions [9, 10, 11, 12, 13].

Theoretical studies of the rotational phenomena in quantum droplets formed by ultracold atoms have already been reported both in the 2D regime [14, 15, 16, 17, 18, 19, 20, 21, 22, 23] and in the 3D regime [24, 25, 26]. In those studies, emphasis is given to the stability—or lack of stability—of optical vortices. As a consequence, in general, an *ansatz* of an order parameter that exhibits such an interesting feature is proposed as an initial state. Then, a dynamical evolution—generated in terms of an extension of the Gross–Pitaevskii equation—is performed. In this work, we take an alternative point of view: we study the dynamics derived from off-axis binary collisions of quantum droplets conformed by mixtures of alkaline atoms that were initially in their corresponding ground states. Up to now, this mechanism has been used to observe the crossover between compressible and incompressible regimes of quantum droplets [27].

Frontal collisions of quantum droplets have already been theoretically analyzed in [28, 29]. Attention was paid to the survival of the quantum droplets as a function of the relative importance of the inertia of the fluid in terms of the initial kinetic energy and its surface tension, i.e., the Weber number [30, 29]. Here, we focus on low-energy collisions.

The initial translational energy is assumed to be controlled by imprinting a specific phase on each otherwise-ground-state droplet; the initial angular momentum requires additional control of the impact parameter.

In the following section, the extended Gross–Pitaevskii equation is written and the general properties of the corresponding ground state are described. An accurate analytical expression for the latter is provided. The initial order parameter is introduced, as well as expressions of the corresponding inertial tensor, translational kinetic energy, Weber number, and linear and angular momenta. Then, we report specific results for the evolution of the dynamical properties of the droplets during binary collisions. We compare the general features of homo- and heteronuclear quantum droplets with parameters that are feasible for experimental realization. Finally, we discuss the main qualitative and quantitative results.

2 Evolution Equation

Consider a mixture of two ultracold Bose gases with atomic masses m_a and m_b , densities n_a and n_b , and scattering lengths $a_{\alpha\beta}$, $\alpha, \beta = a, b$. We assume that the intraspecies scattering lengths $a_{\alpha\alpha} > 0$, while the interspecies scattering length $a_{ab} < 0$. Under the weak coupling condition $na^3 \ll 1$, the long-wavelength instabilities expected from a mean-field theory approach are cured by quantum fluctuations at shorter wavelengths [1, 2]. An expression for those fluctuations was introduced by Lee, Huang, and Yang as a first term in a power-series expansion in the parameter $(na^3)^{1/2}$ for homogeneous quantum fluids [7], and it was extended by Larsen for binary mixtures [8]. An effective formalism that considers finite-range effects was reported in [31]. Looking for a better understanding of the microscopic dynamics, a formalism involving a pairing field has also been developed for homonuclear binary admixtures [32].

The expression of the extended Gross–Pitaevskii equation (EGPE) for the effective order parameters of binary Bose–Bose mixtures Ψ_a used in the present study is [5]

$$i\hbar\partial_t\Psi_\alpha = \left(-\frac{\hbar^2}{2m_\alpha}\nabla^2 + g_{\alpha\alpha}|\Psi_\alpha|^2 + g_{\alpha\beta}|\Psi_\beta|^2 \right) + \frac{4}{3\pi^2}\frac{m_\alpha^{3/5}g_{\alpha\alpha}}{\hbar^3}(m_\alpha^{3/5}g_{\alpha\alpha}|\Psi_\alpha|^2 + m_\beta^{3/5}g_{\beta\beta}|\Psi_\beta|^2)^{3/2}\Psi_\alpha, \quad (1)$$

where the coupling strength factors are defined by $g_{\alpha\beta} = 2\pi\hbar^2 a_{\alpha\beta}/m_{\alpha\beta}$, with $m_{\alpha\beta} = m_\alpha m_\beta / (m_\alpha + m_\beta)$; Ψ_a is normalized to the number of atoms in species a , $N^{(a)}$. This equation results from the Gross–Pitaevskii energy functional for a Bose mixture when both the mean-field term and the LHY correction accounting for quantum fluctuations in the local density approximation are included. The LHY correction involves a dimensionless function [1, 5] $f(z = m_b/m_a, u = g_{ab}^2/(g_{aa}g_{bb}), x = g_{bb}n_b/(g_{aa}n_a)$ that depends on the local density for each atomic species n_a . In Equation (1), this function has been properly parametrized following ref. [5] by the simple expression $(1 + x(m_2/m_1)^{3/5})^{5/2}$ for $u = 1$. The latter effective interaction has been widely discussed [1, 5] and properly describes the general features observed in quantum droplet realizations for both homonuclear [3] and heteronuclear [5] binary Bose–Bose mixtures. For cases in which the relative motion of the components of the droplet can be neglected, e.g., for ground-state calculations, the EGPE acquires a simpler structure [1, 24]. The direction of the separation vector along the direction of the relative momenta of the droplets, and b is the impact parameter which as usual has length units. Here, we work out the evolution of the droplets using Equation (1) since we are especially interested in possible evidence of these otherwise energy-expensive fluctuations.

The parameters

$$\xi_a = \hbar\sqrt{\frac{3}{2}\frac{\sqrt{g_{bb}/m_a} + \sqrt{g_{aa}/m_b}}{|\delta g|\sqrt{g_{aa}n_a^{(0)}}}}, \quad \tau_a = \frac{3\hbar}{2}\frac{\sqrt{g_{aa}} + \sqrt{g_{bb}}}{|\delta g|\sqrt{g_{aa}n_a^{(0)}}}, \quad \delta g = g_{ab} + \sqrt{g_{aa}g_{bb}}. \quad (2)$$

are identified as the natural units of length ξ_a , time τ_a , and δg estimates the degree of balance between the interspecies attraction coupling ($g_{ab} < 0$) and the geometrical average of the intraspecies repulsive coupling. In these equations,

$$n_\alpha^{(0)} = \frac{25\pi}{1024}\frac{1}{(1 + (m_b/m_a)^{3/5}\sqrt{g_{bb}/g_{aa}})^5}\frac{1}{a_{\alpha\alpha}^3}\frac{\delta g^2}{g_{aa}g_{bb}}, \quad (3)$$

yields the expected equilibrium density for $\delta g \ll |g_{ab}|$, $\delta g \ll \sqrt{g_{aa}g_{bb}}$ and a large number of atoms of each species satisfying $N^{(a)}/N^{(b)} = \sqrt{g_{aa}/g_{bb}}$ as obtained in Ref. [1].

Ground State

The self-trapping regime requires a minimum number of atoms N_c . In this regime, the ground state is expected to exhibit [1] (i) the normalized order parameters $(\phi^{(\alpha)} = \Psi_\alpha/\sqrt{N^{(\alpha)}})$ for each component that can be taken as real

and are related by a simple proportionality factor, $\phi_0^{(a)} = \phi_0^{(b)}$; (ii) an asymptotic, $N^{(\alpha)} \rightarrow \infty$, saturation density $n_\alpha^{(0)}$, Equation (3) (in fact, for achieving the quantum droplet regime, it is required that $n_b^{(0)}/n_a^{(0)} \approx \sqrt{g_{aa}/g_{bb}}$); (iii) a spherical shape with radius $R_0 \approx (3N/4\pi n_\alpha^{(0)} \xi^3)^{1/3} \xi$; and (iv) a surface thickness dR of order ξ . The compressible regime corresponds to quantum droplets with a radius R_0 whose value is similar to that of their surface thickness dR .

We have numerically verified [29] that a Boltzmann function

$$\rho_B(r; N) = \frac{A_1}{1 + \exp((r - R_0)N/dR)} \quad (4)$$

accurately describes the ground-state order parameters obtained numerically from Equation (1). The Boltzmann expression allows direct evaluation of the inertial tensor I_{ij} :

$$I_{xx}(N^{(\alpha)}) = I_{yy}(N^{(\alpha)}) = I_{zz}(N^{(\alpha)}) = \frac{8\pi m^{(\alpha)}}{3} \int_0^\infty \rho_B(r; N^{(\alpha)}) r^4 dr \quad (5)$$

$$I_{ij} = 0, i \neq j \quad (6)$$

for each component of a quantum droplet in its ground state.

A study of low-energy excitation with spherical symmetry also yields values of the surface tension both for the incompressible regime

$$\sigma_{incomp}^{(\ell)} = -\frac{\hbar^2 \int dr (\partial_r \phi_0^{(a)})^2 r^{2\ell-2}}{M \int dr \partial_r \rho_0^{(a)} r^{2\ell+1}} \quad (7)$$

and for the compressible regime

$$\sigma_{comp}^{(\ell)} = -\frac{\hbar^2 \int dr (\partial_r \phi_0^{(a)})^2 \int dr \partial_r \rho_0^{(a)} r^{2\ell+1}}{M \left(\int dr \partial_r \rho_0^{(a)} r^{\ell+2} \right)^2} \quad (8)$$

where ℓ is the angular momentum about the symmetry axis of the droplet and $M = (4\pi/3)(m_a m_b / (N^{(a)} m_b + N^{(b)} m_a))$.

3 Binary Collisions of Quantum Droplets

Frontal binary collisions of quantum droplets have been experimentally reported [27]. Those experiments involve two Bose–Einstein condensates confined in a crossed dipole trap with a repulsive thin barrier that splits the BEC along a given horizontal direction. The internal interactions are tuned so that the quantum droplet regime is achieved. Removing the thin barrier and switching off the radial dipole trap, the droplets move towards the center of a vertical levitating trap, acquiring an increasing velocity. After a time interval Δt , the vertical trap is switched off and the two droplets keep moving towards each other. The time interval and the frequency of the radial trap determine the relative momenta of the colliding droplets.

By modifying the geometry of the initial double-well trap, the impact parameter of the droplets can also be controlled. In this section, we study the corresponding low-energy collisions using Equation (1).

Initial State

Consider the collision of quantum droplets that are initially kicked off as described by a plane wave factor $\vec{k}_0 = k_0 \hat{e}_\parallel$ and separated by a vector

$$\vec{d} = 2\vec{d}_0 + b\hat{e}_\perp = 2d_0\hat{e}_\parallel + b\hat{e}_\perp \quad (9)$$

with $\hat{e}_\parallel \cdot \hat{e}_\perp = 0$. That is, $2d_0$ is the initial component of the separation vector along the direction of the relative momenta of the droplets, and b is the impact parameter which as usual has length units. Explicitly,

$$\begin{aligned} \Psi(\vec{r}, t = 0) &= \Psi_1(\vec{r}) + \Psi_2(\vec{r}) \\ &= \begin{pmatrix} \psi_{a_1}(\vec{r} + \vec{d}_0) \\ \psi_{b_1}(\vec{r} + \vec{d}_0) \end{pmatrix} e^{i\vec{k}_0 \cdot \vec{r}/2} + \begin{pmatrix} \psi_{a_2}(\vec{r} - \vec{d}_0 - b\hat{e}_\perp) \\ \psi_{b_2}(\vec{r} - \vec{d}_0 - b\hat{e}_\perp) \end{pmatrix} e^{-i\vec{k}_0 \cdot \vec{r}/2}. \end{aligned} \quad (10)$$

The parameter d_0 is chosen to numerically guarantee a negligible initial overlap of the droplets. At $t = 0$, the mean value

$$\mathcal{K} = -\frac{\hbar^2}{2} \sum_{i=1,2} \int d^3r \Psi_i^\dagger(\vec{r}) \begin{pmatrix} \nabla^2 & 0 \\ 0 & \nabla^2 \end{pmatrix} \Psi_i(\vec{r}), \quad (11)$$

which is a measure of the initial kinetic energy of the droplets, can be decomposed as the sum of the translational kinetic energy of each droplet as a whole \mathcal{K}_{trans} and an internal kinetic energy of the atoms within the droplets \mathcal{K}_{int} . Thus, $\mathcal{K} \approx \mathcal{K}_{trans} + \mathcal{K}_{int}$, with

$$\begin{aligned}\mathcal{K}_{trans} &= \frac{\hbar^2}{2} \left[\frac{N^{(a_1)} k_0^2}{4m_{a_1}} + \frac{N^{(b_1)} k_0^2}{4m_{b_1}} + \frac{N^{(a_2)} k_0^2}{4m_{a_2}} + \frac{N^{(b_2)} k_0^2}{4m_{b_2}} \right], \\ \mathcal{K}_{int} &= -\frac{\hbar^2}{2} \sum_{i=1,2} \sum_{\alpha=a,b} \int d^3r \psi_{\alpha_i}^*(\vec{r}) \frac{\nabla^2}{m_{\alpha_i}} \psi_{\alpha_i}(\vec{r}).\end{aligned}\quad (12)$$

In addition to the impact parameter b , a dimensionless quantity suitable for characterizing binary collisions of classical incompressible droplets, is the Weber number We_ℓ [30]. For each one of the droplets, it is defined as the ratio between the translational kinetic energy \mathcal{K}_{trans} before the collision and the surface energy of excitation evaluated in terms of the surface tension of the droplet; in our case,

$$We_\ell = \frac{\mathcal{K}_{trans}}{R_0^2 \sigma_\ell} \quad (13)$$

where R_0 is the initial radius of the droplet.

For the collision of two identical quantum droplets initially in their ground state internal configuration, this expression becomes

$$We_\ell = \frac{8\pi(dRk_0)^2}{3} \left(\frac{dR}{R_0} \right)^2 \frac{((\ell+2)!)^2}{(2\ell+1)!} \left[1 - \frac{1}{(1+e^{R_0/dR})^2} \right]^{-1} \left[\frac{F_{\ell+1}(R_0/dR)}{F_{2\ell}(R_0/dR)} \right]^2 \quad (14)$$

in the incompressible regime, and

$$We_\ell = \frac{16\pi(dRk_0)^2}{3} \left(\frac{dR}{R_0} \right)^2 (\ell(4\ell^2 - 1)) \frac{F_{2\ell}(R_0/dR)}{F_{2\ell-3}(R_0/dR) + F_{2\ell-4}(R_0/dR)} \quad (15)$$

in the compressible regime. Here, $F_s = (1/\Gamma(s+1)) \int_0^\infty (dx x^s / (1+e^{x-z}))$ denotes the Fermi–Dirac integrals.

We numerically solve Equation (1) with the initial condition Equation (10) by applying the time-evolution operator

$$\Psi(\vec{r}, t + \Delta t) = \exp(-i\mathcal{H}\Delta t/\hbar) \Psi(\vec{r}, t + \Delta t), \quad (16)$$

where \mathcal{H} is identified with the right side of Equation (1). We implemented a Strang decomposition (Split-Step Method), which is accurate to the second order in the time step Δt [33, 34]

$$\exp(-i\mathcal{H}\Delta t/\hbar) \approx \exp(-i\Delta t \mathcal{V}(\vec{r})/(2\hbar)) \exp(-i\Delta t \hat{\mathcal{K}}/\hbar) \exp(-i\Delta t \mathcal{V}(\vec{r})/(2\hbar)). \quad (17)$$

The variable $\hat{\mathcal{K}}$ is the kinetic energy operator from Equation (11), which was evaluated in k -space by means of Fast Fourier transforms (FFTs). The FFT was implemented following [35], and the whole algorithm was developed in Fortran.

4 Evolution of Dynamical Variables during the Collision

The evolution of binary collisions of quantum droplets according to the EGPE equation was numerically evaluated.

The order parameters were obtained both for homonuclear and heteronuclear quantum droplets under feasible experimental conditions. We report results for

- (i) Symmetric $N^{(a)} \approx N^{(b)} = N/2$ mixtures of homonuclear $m_a = m_b$ ^{39}K atoms and scattering lengths compatible with the Feshbach resonances of such atoms: $a_{aa} = a_{bb} = 48.57a_0$, $a_{ab} = -51.86a_0$ [3];
- (ii) Mixtures of ^{41}K and ^{87}Rb [5] with scattering lengths $a_{aa} = 62.0a_0$, $a_{bb} = 100.4a_0$, $a_{ab} = -82.0a_0$. The stability condition $N^{(b)}/N^{(a)} \approx \sqrt{g_{aa}/g_{bb}}$ was imposed.

The number of atoms $N^{(\alpha)}$ was chosen to guarantee the quantum droplet regime and to involve droplets that are expected to exhibit either compressible or incompressible features. To avoid confusion, images and graphs in this section correspond mostly to the same pair—one homonuclear and one heteronuclear—among many studied selections of $N^{(\alpha)}$ for each droplet. A discussion about the main generic findings for other values of $N^{(\alpha)}$ not explicitly shown in the figures is given at the end of this section.

In [29], the values of the parameters A_1 , R_0 , and dR necessary to obtain an expression for the ground-order parameter using Equation (4) are given so that the initial state Equation (10) has an analytical representation. We used $\hat{e}_{\parallel} = (1/\sqrt{3})(1, 1, 1)$ and $\hat{e}_{\perp} = 1/\sqrt{2}(-1, 1, 0)$ in the numerical simulations.

In all the cases that we explored, the resulting evolution of the atomic densities for the different atomic species maintain, within numerical accuracy, the same proportionality factor. That is, we numerically found that during the evolution,

$$\rho_a(\vec{r}, t) = \Psi_a^*(\vec{r}, t)\Psi_a(\vec{r}, t) = \frac{N^{(a)}}{N^{(b)}}\Psi_b^*(\vec{r}, t)\Psi_b(\vec{r}, t) = \frac{N^{(a)}}{N^{(b)}}\rho_b(\vec{r}, t) \quad (18)$$

$$\Psi_{\alpha}(\vec{r}, t) = \psi_{\alpha_1}(\vec{r}, t) + \psi_{\alpha_2}(\vec{r}, t), \quad \alpha = a, b \quad (19)$$

$$N^{(\alpha)} = N^{(\alpha_1)} + N^{(\alpha_2)} \quad (20)$$

where α_k , $k = 1, 2$ enumerate the two colliding droplets. Illustrative examples are depicted in Figure 1.

However, when the overlap between the order parameters is estimated using the fidelity F

$$F(t) = \frac{|\langle \Psi_a(t) | \Psi_b(t) \rangle|^2}{\|\Psi_a(t)\|^2 \|\Psi_b(t)\|^2}, \quad \|\Psi_a(t)\|^2 = \langle \Psi_a(t) | \Psi_a(t) \rangle \quad (21)$$

as a figure of merit, it is found to exhibit a nontrivial evolution for heteronuclear droplets and $b \neq 0$, while it equals unity for the collision of homonuclear droplets, as exemplified in Figure 2. The order parameters are normalized to the total number of atoms in the corresponding species $\|\Psi_{\alpha}(t)\|^2 = N^{(\alpha)}$, which in this work we take as constant. This assumption prevents the validity of our calculations for long times compared to those yielding significant atomic losses [4, 5, 27, 29].

A local comparison of the order parameters was also performed in terms of the real and imaginary parts of the fidelity density

$$\mathcal{F}(\vec{r}, t) = \frac{\Psi_a^*(\vec{r}, t)\Psi_b(\vec{r}, t)}{\|\Psi_a(t)\| \|\Psi_b(t)\|}, \quad (22)$$

which is also illustrated in Figure 1.

Since the densities associated with the order parameters $\Psi_{\alpha}(\vec{r}, t)$ are equal, $F(t) \neq 1$ implies that different phases were acquired during the collision.

Since the densities for each atomic species are equal through the collision, the inertia tensors

$$\bar{I}_{ij}^{(\alpha)}(t) = m_{\alpha} \int d^3r \Psi_{\alpha}^*(\vec{r}, t) r_i r_j \Psi_{\alpha}(\vec{r}, t) \quad (23)$$

differ only by a proportional constant given by the ratio of the total mass of each species in the two droplets: $m_a N^{(a)} / m_b N^{(b)}$.

The diagonalization of $\bar{I}_{ij}^{(\alpha)}(t)$ allows identification of the principal axes at each time. The behavior of the direction of the eigenvector corresponding to the largest eigenvalue of the diagonalized $\bar{I}_{ij}^{(\alpha)}(t)$ allows a schematic view of the rotation of the atomic cloud. This is illustrated in Figure 3. For simplicity, we report $\bar{I}^{(\alpha)}$ divided by the total mass $m_{\alpha} N^{(\alpha)}$. The initial value depends directly on the impact parameter. The long-time evolution of the illustrated eigenvector could also be used to identify a quasiperiodic global rotation of the coalesced quantum droplet. The illustrative example in Figure 3 considers the same impact parameter and different kinetic factors k_0 . For the same kinetic factors, differences in the evolution of homonuclear and heteronuclear maximum eigenvalues and eigenvectors are still observable but are less evident than expected.

We also evaluated the evolution of the linear

$$\vec{P} = -i\hbar \sum_{\alpha=a,b} \int d^3r \Psi_{\alpha}^{\dagger}(\vec{r}) \vec{\nabla} \Psi_{\alpha}(\vec{r}) \quad (24)$$

$$= N^{(a)} \vec{P}^{(a)} + N^{(b)} \vec{P}^{(b)} \quad (25)$$

$$\vec{P}^{(\alpha)} = -\frac{i\hbar}{N^{(\alpha)}} \int d^3r [(\psi_{\alpha_1}^*(\vec{r}, t) + \psi_{\alpha_2}^*(\vec{r}, t)) \vec{\nabla} (\psi_{\alpha_1}(\vec{r}, t) + \psi_{\alpha_2}(\vec{r}, t))], \quad (26)$$

and angular momenta

$$\vec{L} = -i\hbar \sum_{\alpha=a,b} \int d^3r \Psi_{\alpha}^{\dagger}(\vec{r}) \vec{r} \times \vec{\nabla} \Psi_{\alpha}(\vec{r}) \quad (27)$$

$$= N^{(a)} \vec{L}^{(a)} + N^{(b)} \vec{L}^{(b)} \quad (28)$$

$$\vec{L}^{(\alpha)} = -\frac{i\hbar}{N^{(\alpha)}} \int d^3r [(\psi_{\alpha_1}^*(\vec{r}, t) + \psi_{\alpha_2}^*(\vec{r}, t)) \vec{r} \times \vec{\nabla} (\psi_{\alpha_1}(\vec{r}, t) + \psi_{\alpha_2}(\vec{r}, t))], \quad (29)$$

in terms of the corresponding dynamical densities per number of atoms of each of the two species.

The total linear and angular momentum during the collision is expected—and numerically confirmed—to be conserved. For heteronuclear droplets, the differences in the phases of the order parameters necessarily leads to differences in the linear and angular momentum for each atomic species. In Figures 4-5, the differences are illustrated as a function of the impact parameter b and the kinetic factor k_0 . As expected, these differences are greater for smaller values of b and a given k_0 . The lightest atoms are more susceptible to the collision effects.

Up to now, the numerical results explicitly reported in the Figures correspond to binary off-axis collisions of droplets that differ in the number of atoms in each initial droplet, with both being close to the boundary between the incompressible and compressible regimes. In the case of identical incompressible droplets formed by heteronuclear droplets, the behavior of the difference in the angular momentum for heteronuclear mixtures is similar to that of different incompressible droplets. That is not the case for one droplet in the incompressible regime and the other in the compressible regime. Our numerical simulations indicate that these differences are smaller; the reason can be attributed to a soft coalescence of the two droplets that allows both species to attain more-similar phases based on their respective order parameters.

Let us compare the behavior of the dynamical variables for different collisions. We focus on the time average of the angular momentum vector, and we define

$$\Delta L_k(N_1, N_2; N'_1, N'_2) = \frac{\langle L_k^{(a)}(N_1, N_2) - L_k^{(b)}(N_1, N_2) \rangle_t}{\langle L_k^{(a)}(N'_1, N'_2) - L_k^{(b)}(N'_1, N'_2) \rangle_t}, \quad k = x, y, z \quad (30)$$

where the pair (N_1, N_2) allows for identification of the quantum droplet ground states in a collision. For instance, the collision of two identical droplets corresponds to $N_1^{(Rb)} = N_2^{(Rb)}$. For the heteronuclear droplets under consideration we take $N_1^{(K)} = N_1^{(Rb)}/1.15$.

We now compare collisions involving identical droplets, identified by $N_1^{(\alpha)}$, to collisions where the number of atoms $N_2^{(\alpha)}$ in just one of the droplets has been modified. For given values of the impact parameter b and the kinetic parameter k_0 , we find numerically that

$$\Delta L_k(N_1, N_2; N_1, N_1) = \frac{\langle L_k^{(K)}(N_1, N_2) - L_k^{(Rb)}(N_1, N_2) \rangle_t}{\langle L_k^{(K)}(N_1, N_1) - L_k^{(Rb)}(N_1, N_1) \rangle_t}, \quad k = x, y, z \quad (31)$$

depends on N_1 and N_2 but is almost independent of b and k_0 within the range of parameters reported in this work. In fact, this ratio seems to be simply related to the quotient of the Weber number

$$\Delta L_k(N_1, N_2; N_1, N_1) \approx \frac{(N_2^{(Rb)} + N_2^{(K)}) \text{We}(N_2)}{(N_1^{(Rb)} + N_1^{(K)}) \text{We}(N_1)}. \quad (32)$$

This finding is illustrated in Figure 6. There, we report $\Delta \vec{L}(N_1, N_2; N_1, N_1)$ for nine pair-collision parameters (b, k_0) that were used in the illustrative examples in Figures 4 and 5. The corresponding value of the Weber number We as a function of the number of atoms for the ground state was calculated directly from Equations (14) and (15) and results in the numbers reported in Table 1. The evolution of the 27 collisions using the EGPE allowed the calculation of the corresponding difference in angular momenta for the atoms in each species. It was then averaged over time. This results in a simple relation between both independent calculations, given by Equation (32). A clear phenomenological connection between these numerical findings and the dynamics induced by the EGPE remains to be explored.

The interesting correlation between the differentiated dynamics of each atomic species and the Weber number indicates that—similarly to the classical analogue—the expectations for the dynamical evolution of the collision would be better described by providing both the Weber number (instead of the initial translation energy) and the impact parameter.

Table 1: Radius of ground-state droplet R_0 for a mixture of Rb and K atoms interacting with the scattering lengths mentioned in the main text. The scaled Weber number is related to the actual quadrupolar ($\ell = 2$) one by the expression $We = \widetilde{We} k_0^2$. N_c is the critical number of rubidium atoms required to reach the quantum droplet regime for the interaction strengths of the heteronuclear atoms considered in this work.

| $N^{(Rb)}$ | R_0 [μm] | \widetilde{We} |
|--------------------|-------------------------|------------------|
| 96818 = 7.64 N_c | 3.36 | 2.50 |
| 70227 = 5.54 N_c | 2.97 | 3.17 |
| 37000 = 2.9 N_c | 2.31 | 3.40 |

5 Conclusions

Binary collisions of quantum droplets are an ideal scenario for studying the dynamics of quantum degenerate gases without confining potentials. In this work, we have studied theoretically the behavior of the elementary kinematic and dynamical variables of droplets formed by binary mixtures of homonuclear and heteronuclear droplets. Low-energy off-axis collisions involve both nontrivial rotational and translational evolution. For the parameters reported here, the evolved dilute degenerate gas seems to result from the coalescence of the initial individual droplets. The coalesced droplet rotates as a whole for times long enough to admit an experimental corroboration. It is found that the density of the individual atom species is the same during the process, while the phase of the corresponding order parameters differs. Direct consequences of this behavior are predicted on the linear and angular momenta; the differences reflected by ct parameter and seem to be determined by the relation between the translational energy and the surface tension, i.e., the Weber number, in an amazingly simple way that deserves further analysis.

The experimental observation of the dynamics of quantum droplets before and after a collision is highly constrained by atomic losses. Self-evaporation and three-body scattering have been identified as relevant atomic loss mechanisms [4, 5, 27, 29]. In this work, we report calculations before atomic losses are expected to be significant. The possibility of vortex formation via this excitation method is not excluded, but given the energies involved in this kind of collision, it seems not to be a dominant effect. Both issues—long-time evolution and vortex generation—require further studies involving a larger parameter space. The possibility of controlling differentiated dynamics of atomic species via binary collisions is an interesting prediction derived from the simulations reported in this work.

References

- [1] Petrov, D.S. Quantum mechanical stabilization of a collapsing Bose-Bose mixture. *Phys. Rev. Lett.* **2015**, *115*, 155302.
- [2] Petrov, D.S.; Astrakharchik, G.E. Ultradilute low-dimensional liquids. *Phys. Rev. Lett.* **2016**, *117*, 100401.
- [3] Cabrera, C. R.; Tanzi, L.; Sanz, J.; Naylor, B.; Thomas, P.; Cheiney, P.; Tarruell L. Quantum liquid droplets in a mixture of Bose-Einstein condensates. *Science* **2017**, *359*, 301.
- [4] Semeghini, G.; Ferioli, G.; Masi, L.; Mazzinghi, C.; Wolswijk, L.; Minardi, F.; Modugno, M.; Modugno, G.; Inguscio, M.; Fattori, M. Self-bound quantum droplets of atomic mixtures in free space. *Phys. Rev. Lett.* **2018**, *120*, 235301.
- [5] D’Errico, C.; Burchianti, A.; Prevedelli, M.; Salasnich, L.; Ancilotto, F.; Modugno, M.; Minardi, F.; Fort, C. Observation of quantum droplets in a heteronuclear bosonic mixture, *Phys. Rev. Res.* **2019**, *1*, 033155.
- [6] Guo, Z.; Jia, F.; Li, L.; Ma, Y.; Hutson, J.M.; Cui, X.; Wang, D. Lee-Huang-Yang effects in the ultracold mixture of ^{23}Na and ^{87}Rb with attractive interspecies interactions, *Phys. Rev. Res.* **2021**, *3*, 033247.
- [7] Lee, T.D.; Huang, K.; Yang, C.N. Eigenvalues and eigenfunctions of a Bose system of hard spheres and its low-temperature properties. *Phys. Rev.* **1957**, *106*, 1135.
- [8] Larsen, D.M. Binary mixtures of dilute Bose gases with repulsive interactions at low temperature. *Ann. Phys.* **1963**, *24*, 89.
- [9] Ferrier-Barbut, I.; Kadau, H.; Schmitt, M.; Wenzel, M.; Pfau, T. Observation of quantum droplets in a strongly dipolar Bose gas. *Phys. Rev. Lett.* **2016**, *116*, 215301.
- [10] Schmitt, M.; Wenzel, M.; Böttcher, F.; Ferrier-Barbut, I.; Pfau, T. Self-bound droplets of a dilute magnetic quantum liquid. *Nature* **2016**, *539*, 259.

- [11] Chomaz, L.; Baier, S.; Petter, D.; Mark, M.J.; Wächtler, F.; Santos, L.; Ferlaino, F. Quantum-fluctuation-driven crossover from a dilute Bose-Einstein condensate to a macrodroplet in a dipolar quantum fluid. *Phys. Rev. X* **2016**, *6*, 041039.
- [12] Tanzi, L.; Lucioni, E.; Famà, F.; Catani, J.; Fioretti, A.; Gabbanini, C.; Bisset, R.N.; Santos, L.; Modugno, G. Observation of a dipolar quantum gas with metastable supersolid properties. *Phys. Rev. Lett.* **2019**, *122*, 130405.
- [13] Böttcher, F.; Wenzel, M.; Schmidt, J.N.; Guo, M.; Langen, T.; Ferrier-Barbut, I.; Pfau, T.; Bombín, R.; Sánchez-Baena, J.; Boronat, J.; et al. Dilute dipolar quantum droplets beyond the extended Gross-Pitaevskii equation. *Phys. Rev. Res.* **2019**, *1*, 033088.
- [14] Fetter, A.L. Rotating trapped Bose-Einstein condensates. *Rev. Mod. Phys.* **2009**, *81*, 647.
- [15] Malomed, B.A. Vortex solitons: Old results and new perspectives. *Phys. D* **2019**, *399*, 108.
- [16] Kartashov, Y.V.; Malomed, B.A.; Torner, L. Metastability of. Quantum Droplet Clusters. *Phys. Rev. Lett.* **2019**, *122*, 193902.
- [17] Luo, Z.-H.; Pang, W.; Liu, B.; Li, Y.-Y.; Malomed, B.A. A new form of liquid matter: Quantum droplets. *Front. Phys.* **2021**, *16*, 32201.
- [18] Li, Y.; Chen, Z.; Luo, Z.; Huang, C.; Tan, H.; Pang, W.; Malomed, B.A. Two-dimensional vortex quantum droplets. *Phys. Rev. A* **2018**, *98*, 063602.
- [19] Examilioti, P.; Kavoulakis, G.M. Ground state and rotational properties of two-dimensional self-bound quantum droplets. *J. Phys. B* **2020**, *53*, 175301.
- [20] Tengstrand, M.N.; Stürmer, P.; Karabulut, E.Ö.; Reimann, S.M. Rotating binary Bose-Einstein condensates and vortex clusters in quantum droplets. *Phys. Rev. Lett.* **2019**, *123*, 160405.
- [21] Stürmer, P.; Tengstrand, M.N.; Sachdeva, R.; Reimann, S.M. Breathing mode in two-dimensional binary self-bound Bose-gas droplets. *Phys. Rev. A* **2021**, *103*, 053302.
- [22] Kartashov, Y.V.; Malomed, B.A.; Torner, T. Structured heterosymmetric quantum droplets. *Phys. Rev. Research* **2020**, *2*, 033522.
- [23] Otajonov, S.R.; Tsoy, E.N.; Abdullaev F.K. Variational approximation for two-dimensional quantum droplets. *Phys. Rev. E* **2020**, *102*, 062217.
- [24] Kartashov, Y.V.; Malomed, B.A.; Tarruell, L.; Torner, L. Three-dimensional droplets of swirling superfluids. *Phys. Rev. A* **2018**, *98*, 013612.
- [25] Ancilotto, F.; Barranco, M.; Guilleumas, M.; Pi, M. Self-bound ultradilute Bose mixtures within local density approximation. *Phys. Rev. A* **2018**, *98*, 053623.
- [26] Caldara, M.; Ancilotto, F. Vortices in quantum droplets of heteronuclear Bose mixtures. *Phys. Rev. A* **2022**, *105*, 063328.
- [27] Ferioli, G.; Semeghini, G.; Masi, L.; Giusti, G.; Modugno, G.; Inguscio, M.; Gallelli, A.; Recati, A.; Fattori, M. Collisions of Self-Bound Quantum Droplets. *Phys. Rev. Lett.* **2019**, *122*, 090401.
- [28] Cikojević, V.; Vranješ Markić, L.; Pi, M.; Barranco M.; Ancilotto, F.; Boronat, J. Dynamics of equilibration and collisions in ultradilute quantum droplets. *Phys. Rev. Res.* **2021**, *3*, 043139.
- [29] Alba-Arroyo, J.E.; Caballero-Benitez, S.F.; Jáuregui, R. Weber number and the outcome of binary collisions between quantum droplets. *Sci. Rep.* **2022**, *12*, 18467.
- [30] Frohn, A.; Roth, N. *Dynamics of Droplets*; Springer Science and Business Media: Berlin/Heidelberg, Germany, 2000.
- [31] Cikojević, V.; Džalilija, K.; Stipanović, P.; Vranješ Markić L.; Boronat, J. Ultradilute quantum liquid drops. *Phys. Rev. B* **2018**, *97*, 140502.
- [32] Hu, H.; Liu, X.J. Microscopic derivation of the extended Gross-Pitaevskii equation for quantum droplets in binary Bose mixtures. *Phys. Rev. A* **2020**, *102*, 043302.
- [33] Strang, G. On the construction and comparison of difference schemes. *SIAM J. Numer. Anal.* **1968**, *5*, 506.
- [34] Bao, W.; Jaksch, D.; Markowich, P.A. Numerical solution of the Gross-Pitaevskii equation for Bose-Einstein condensation. *J. Comp. Phys.* **2003**, *187*, 318.
- [35] Press, W.H. *Numerical Recipes in Fortran 77: The Art of Scientific Computing*, 2nd ed.; University of Cambridge: Cambridge, UK, 1992.

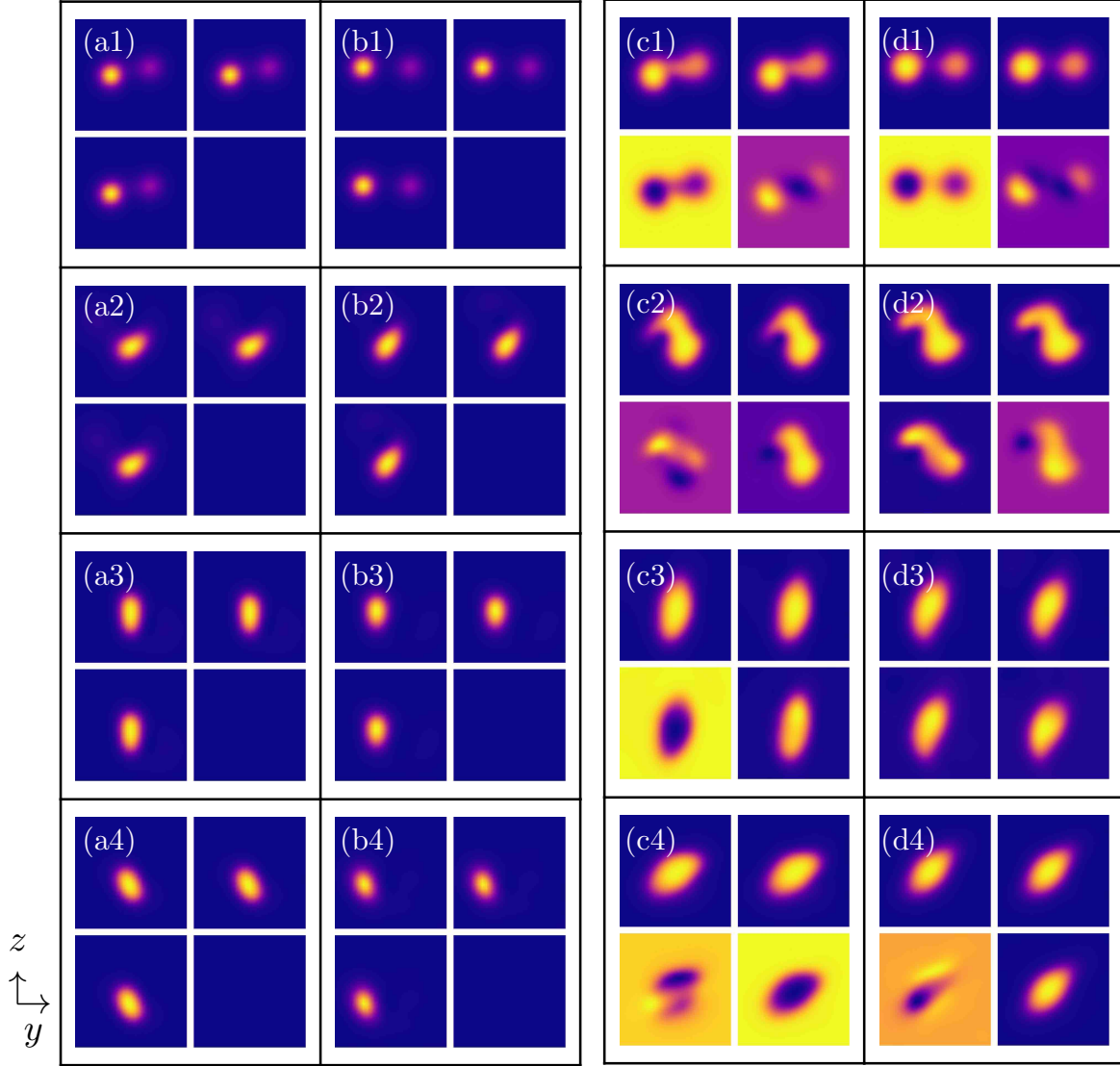


Figure 1: Comparative illustrations of the evolution of the (odd rows) atomic density and of the (even rows) fidelity of the (a,b) homonuclear and (c,d) heteronuclear (left) real part and (right) imaginary part of two quantum droplets in a binary collision. The adjacent columns of the density for a given letter correspond to different atomic species. The numbering (e.g., **a1**, **a2**, **a3**, and **a4**) indicates different equidistant times. The adjacent columns of the fidelity density refer to the real and imaginary parts as defined by Equation (22). In the homonuclear case, $N_1^{(K)} = 79,979$, and $N_2^{(K)} = 110,011$ for the second one. In the heteronuclear case, $N_1^{(Rb)} = 70,227$, $N_2^{(Rb)} = 96,818$, and $N_i^{(Rb)}/N_i^{(K)} = 1.15$ for the second one. The kinetic parameter is $k_0 = 11 \mu\text{m}^{-1}$. The snapshots correspond to the following evolution times: (a1,b1): 6.3662 ms, (a2,b2): 12.7324 ms, (a3,b3): 19.0986 ms, and (a4,b4): 25.4648 ms for the homonuclear panels and (c1,d1): 9.5493 ms, (c2,d2): 15.9155 ms, (c3,d3): 22.2817 ms, and (c4,d4): 28.6479 ms for the heteronuclear panels. The impact parameters for panels (a,c) $b = 2$ and for (b,d) $b = 3$ in units of $0.855 \mu\text{m}$. All graphs depict the behavior at the y - z plane.

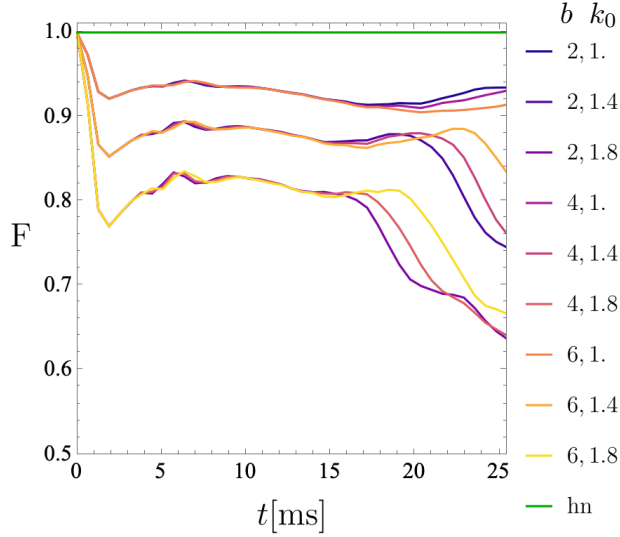


Figure 2: Evolution of the fidelity F for two heteronuclear quantum droplets in a binary collision. In this illustrative example, $N_1^{(K)} = 70,227$, $N_2^{(K)} = 96,818$, and $N_i^{(Rb)}/N_i^{(K)} = 1.15$. Different impact parameters b and kinetic factors k_0 are considered; the unit of length is $0.855 \mu\text{m}$, so that k_0 is given in units of $7.35 \mu\text{m}^{-1}$.

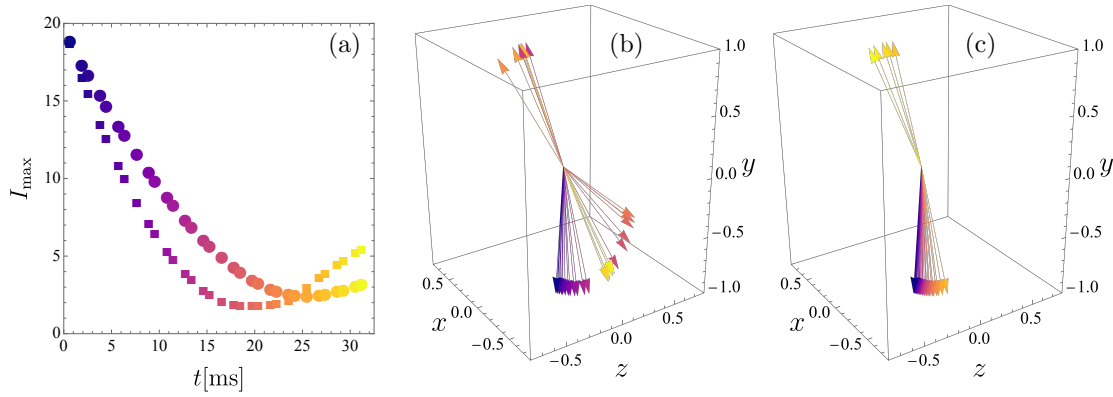


Figure 3: Evolution of (a) the largest eigenvalue of the inertia tensor $\bar{I}_{ij}^{(\alpha)}(t)/m_\alpha N^{(\alpha)}$ and the corresponding eigenvector for (b) a homonuclear ($N_1^{(K)} = 79,979$ and $N_2^{(K)} = 110,011$) and (c) a heteronuclear ($N_1^{(Rb)} = 70,227$, $N_2^{(Rb)} = 96,818$, and $N_i^{(Rb)}/N_i^{(K)} = 1.15$) mixture. In (a), circles correspond to the heteronuclear case and squares to the homonuclear case. The unit of length is $0.855 \mu\text{m}$. In this illustrative example, the two homonuclear droplets collide with $b = 3.42 \mu\text{m}$ and $k_0 = 14.7 \mu\text{m}^{-1}$, while $b = 3.42 \mu\text{m}$ and $k_0 = 7.35 \mu\text{m}^{-1}$ for the heteronuclear case. The color of each vector in (b) and (c) allows the identification of the evolution time using the (a) panel.

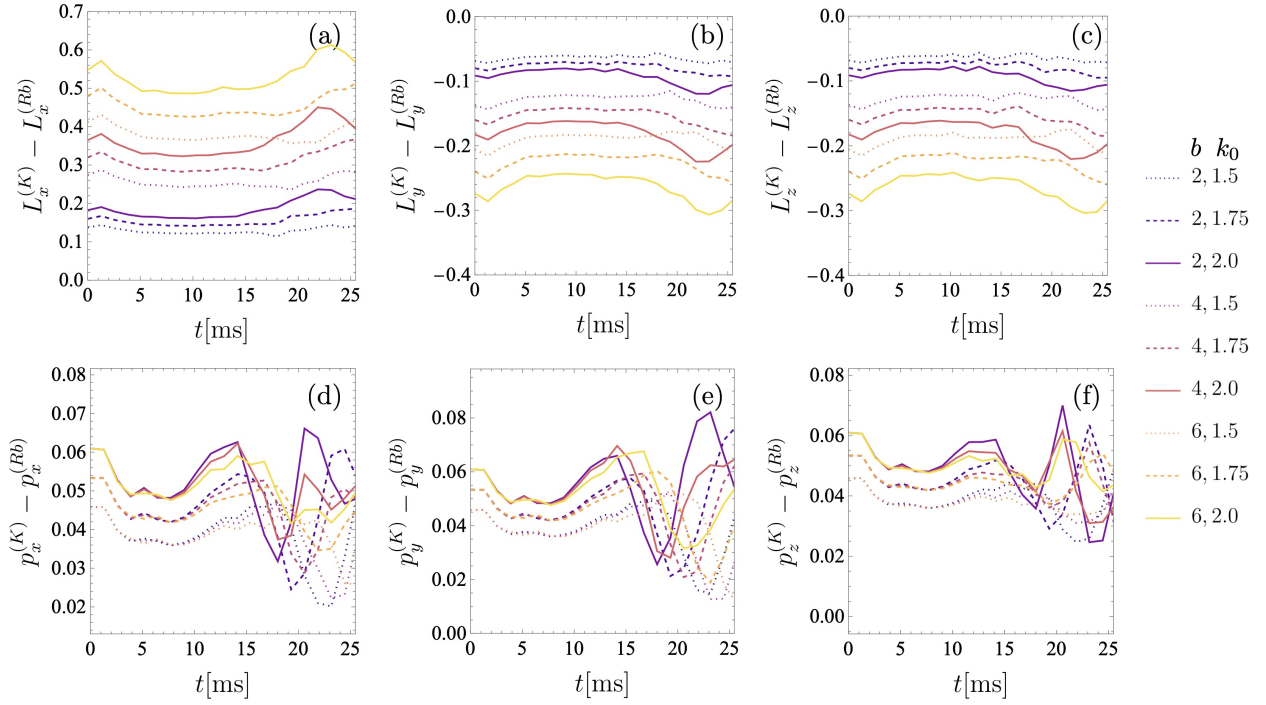


Figure 4: Evolution of the difference of the angular momentum (a-c) and linear (d-f) vector components per atom for two heteronuclear quantum droplets in a binary collision; $N_1^{(Rb)} = 70,227$, $N_2^{(Rb)} = 96,818$, and $N_i^{(Rb)}/N_i^{(K)} = 1.15$. Different impact parameters b and kinetic factors $\hbar k_0$ are considered; the length unit is $0.855 \mu\text{m}$, so that k_0 is given in units of $7.35 \mu\text{m}^{-1}$. The angular momentum per atom is given in units of \hbar .

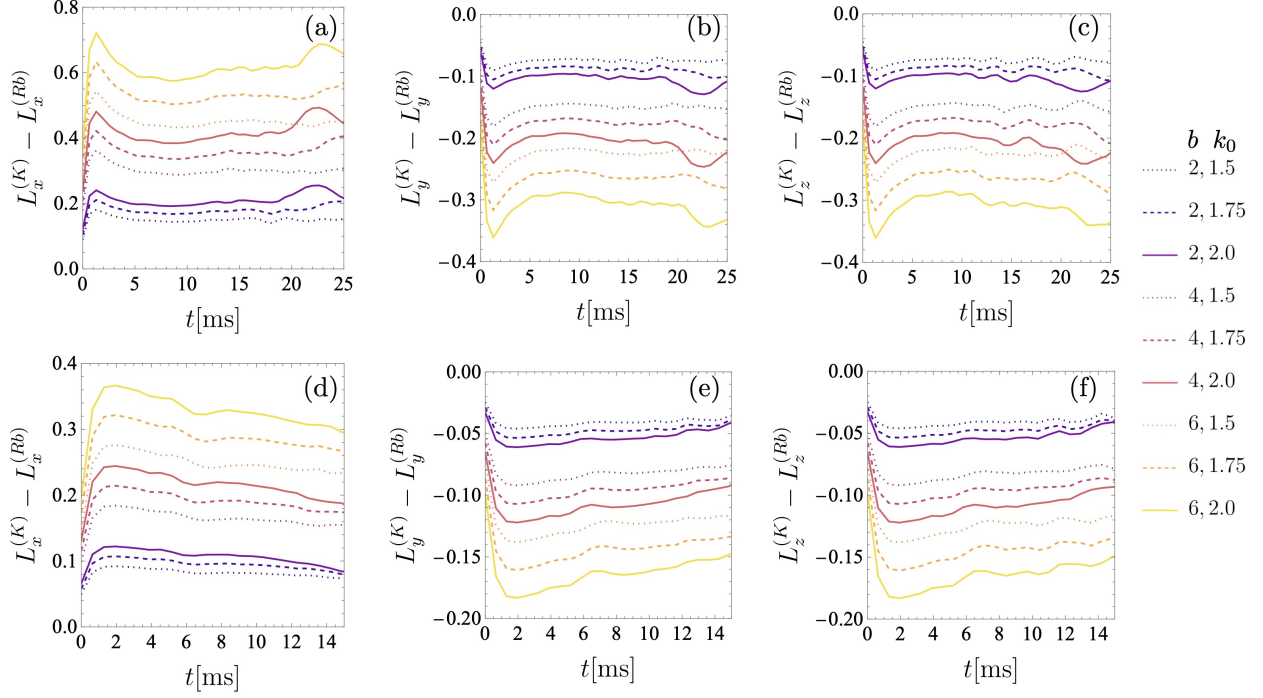


Figure 5: Evolution of the difference of the angular momentum vector components per atom for two heteronuclear quantum droplets in a binary collision. In the first row (a-c), the droplets are initially identical and $N_1^{(Rb)} = N_2^{(Rb)} = 96,818$; in the second row (d-f), $N_1^{(Rb)} = 37,000$ and $N_2^{(Rb)} = 96,818$, with $N_i^{(Rb)}/N_i^{(K)} = 1.15$. The length unit is $0.855 \mu\text{m}$, so that k_0 is given in units of $7.35 \mu\text{m}^{-1}$. Angular momentum per atom is measured in \hbar units.

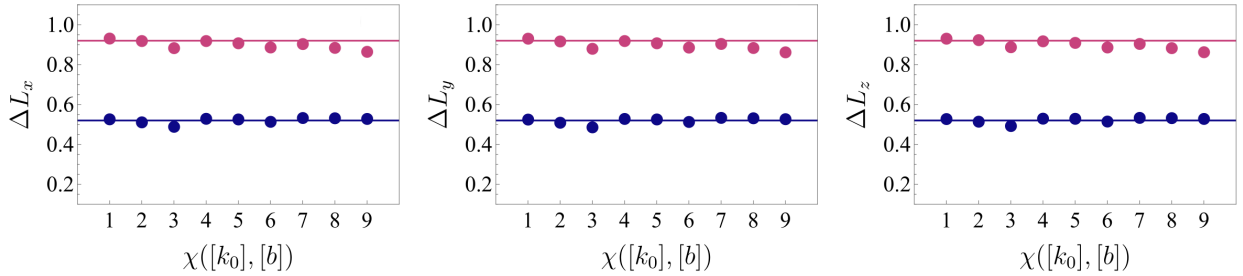


Figure 6: Ratio of the time average of the difference of the angular momentum components for the two atomic species $\Delta L_k(N_1, N_2; N_1, N_1)$, Equation (31). In these cases $N_1^{(Rb)} = 96,818$, $N_2^{(Rb)} = 70,227$ (magenta circles), and $N_2^{(Rb)} = 37,000$ (blue circles). The values of $[b] = 2, 4, 6$ and $[k_0] = 1.5, 1.75, 2.0$ should be directly substituted in the expression $\chi([k_0], [b]) = [b]/2 + 12([k_0] - 3/2)$ to identify the abscissa. The corresponding value of the Weber number We as a function of the number of particles can be evaluated using Table 1.